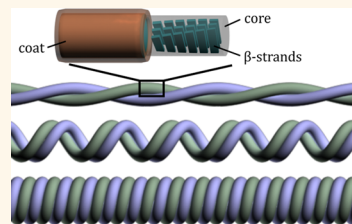


# Correlation between Nanomechanics and Polymorphic Conformations in Amyloid Fibrils

Ivan Usov and Raffaele Mezzenga\*

Food & Soft Materials Science, Department of Health Science & Technology, ETH Zurich, Schmelzbergstrasse 9, LFO E23, 8092 Zurich, Switzerland

**ABSTRACT** Amyloid fibrils occur in diverse morphologies, but how polymorphism affects the resulting mechanical properties is still not fully appreciated. Using formalisms from the theory of elasticity, we propose an original way of averaging the second area moment of inertia for non-axisymmetric fibrils, which constitutes the great majority of amyloid fibrils. By following this approach, we derive theoretical expressions for the bending properties of the most common polymorphic forms of amyloid fibrils (twisted ribbons, helical ribbons, and nanotubes), and we benchmark the predictions to experimental cases. These results not only allow an accurate estimation of the amyloid fibrils' elastic moduli but also bring insight into the structure–property relationships in the nanomechanics of amyloid systems, such as in the closure of helical ribbons into nanotubes.



**KEYWORDS:** amyloid fibrils · polymorphism · nanomechanics

The formation of amyloid fibrils *in vivo* has implications in neurodegenerative disorders such as Alzheimer's or Parkinson's diseases<sup>1–7</sup> and hence has a tremendous relevance in medical research. Nonetheless, amyloid fibrils formed from various polypeptides and hydrolyzed proteins start to be recognized also as an important class of bio-nanomaterials<sup>8,9</sup> or as efficient building blocks for functional materials.<sup>10–12</sup> Irrespective of the particular polymorphic form in which amyloid fibrils occur, they all share a common fingerprint at the molecular level: the cross- $\beta$  structure.<sup>13</sup> The large interaction energy between  $\beta$ -strands and  $\beta$ -sheets, arising from hydrogen bonds and hydrophobic forces, provides these systems with a remarkably large elastic modulus and strength.<sup>14</sup> Beside the main load-carrying cross- $\beta$  structure, amyloid fibrils can also be covered by a coat of unstructured polypeptide chains (Figure 1a),<sup>15</sup> which has been particularly well-described in the case of the tau protein.<sup>16</sup> An interaction between side chains in this coat might also have an influence on the final mechanical properties of fibrils.<sup>17</sup>

Understanding the physical properties of amyloid fibrils is central for the rationalization of their implications in neurodegenerative diseases, their growth to amyloid plaques, and the biophysical processes

involved in protein misfolding. Despite the importance of this topic, however, a general approach capable of extracting intrinsic physical properties of amyloid fibrils, such as the Young's (elastic) modulus, from both observable structural features (e.g., persistence length) and topological details (polymorphic forms) is not yet available. Here we present the first general approach based on elasticity theory allowing disentangling of the intrinsic rigidity of amyloid fibrils from the different polymorphic forms in which these fibrils can occur. Even within the same protein precursor, the amyloid system can exhibit several pathways of polymorphic transition;<sup>18</sup> however, the most predominant evolution is the transformation from twisted ribbons to nanotubes *via* a helical ribbon state, which was identified in many amyloid systems.<sup>19–24</sup> An example of fibrils from bovine serum albumin (BSA) protein source is shown in Figure 1b–d. In what follows, we first derive new theoretical expressions for the bending properties of amyloid fibrils as a function of their morphology, and we then benchmark the predicted elastic moduli to experimental values extracted by nanoindentation in systems exhibiting the three most common forms of polymorphisms, such as twisted ribbons, helical ribbons, and nanotubes. The assumption of isotropic material is needed to make

\* Address correspondence to raffaele.mezzenga@hest.ethz.ch.

Received for review June 30, 2014 and accepted October 2, 2014.

Published online October 02, 2014  
10.1021/nn503530a

© 2014 American Chemical Society

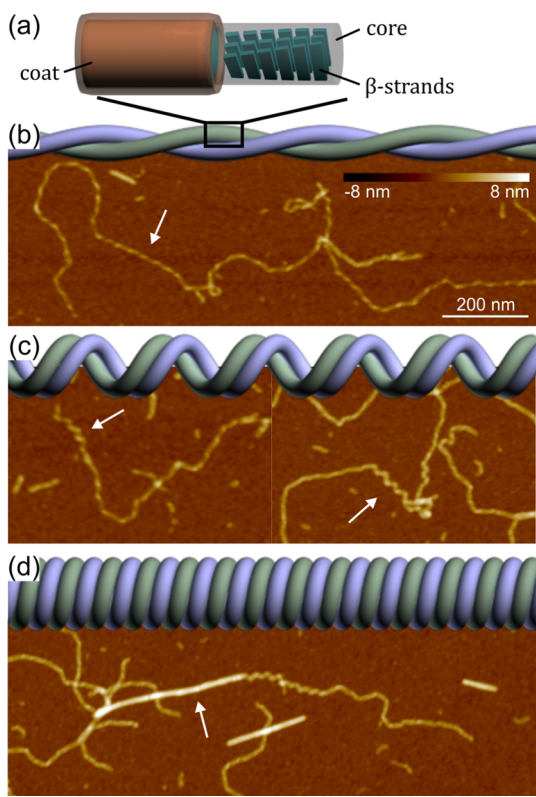


**Figure 1.** (a) Schematic view of the internal cross- $\beta$  structure of a protofilament. Different polymorphic types of an amyloid fibril composed of two protofilaments and, as an example, corresponding AFM images of fibrils from BSA possessing these conformations: (b) twisted ribbon, (c) helical ribbon, and (d) closed nanotube.

possible all derivations presented in this article. There is, however, a possibility that amyloid fibrils possess some level of anisotropy and, therefore, a different elastic response in the axial and radial directions, that is, slightly different values of longitudinal and transversal moduli.<sup>25</sup> Yet, due to limited differences between longitudinal and transversal moduli, the comparison between elastic properties along different directions remains appropriate, and results from nanoindentation remain the most robust experimental benchmark available to date. We note here that the nanoindentation results discussed in this work have already been validated against corrections for substrate and cantilever tip radii by performing nanoindentation experiments on thick, homogeneous films of amyloid fibrils, for which both tip radii and substrate effects become irrelevant.<sup>26</sup>

The general approach followed to determine the nanomechanical properties of the fibrils is to calculate the elastic strain energy stored in a bended fibril of a given polymorphism and derive the characteristics of an equivalent simple beam storing the same elastic strain energy and carrying the same bending moment.<sup>27</sup> Typically, assumptions on the cross section are made to enable the use of affordable estimations of  $I$ . This can be ambiguous for non-axisymmetric geometries.

Our approach provides a general toolbox for the correct estimation of  $I$  starting from energy density equations of general validity in continuum mechanics and thus can be applied to any specific geometry. Amyloid systems studied in this work are BSA,<sup>18,28</sup>  $\beta$ -lactoglobulin,<sup>29,30</sup> and the end-capped heptapeptide  $\text{CH}_3\text{CONH-}\beta\text{A-}\beta\text{AKLVFF-CONH}_2$ , modified from the  $\text{A}\beta(16-20)$  fragment KLVFF.<sup>19,31</sup> The findings presented in the current study are general because they are derived by principal elasticity theory arguments and thus can also be applied to collagen, microtubules, fibronectin, or any other type of fibrous objects.

## RESULTS AND DISCUSSION

**Bending of a Twisted Ribbon.** The general formula for the strain energy  $U$  stored in an elongated object, is

$$U = \frac{M^2 L}{2D} \quad (1)$$

where  $M$  is a bending moment,  $L$  is a length of an object, and  $D$  is a bending (flexural) rigidity (see Supporting Information). For a simple prismatic beam of any type of cross section with a longitudinal plane of symmetry and bending moment  $M$  acting in the  $xz$  plane,  $D = EI_y$ , where  $E$  is a Young's (elastic) modulus and  $I_y$  is an area moment of inertia (second moment of area) with respect to a neutral  $y$  axis (see eq S2). Generally,  $D$  can be expressed as a function of the material mechanical properties and object geometry, hence  $D = D(E, G, I_x, I_y, I_z, \alpha_i)$ , where  $G$  is a shear modulus of a material and a set  $\alpha_i$  represents generalized geometrical parameters of the system.

To illustrate the generality of eq 1, we proceed to the different polymorphic forms, starting from the twisted ribbons. This shape is relatively similar to a rectangular beam, with the only difference being a periodical variation in cross section and hence in the local area moment of inertia. An expected result would have to be  $D = E\langle I \rangle$ , with  $\langle I \rangle$  being an effective second moment of area, from a suitable averaging (to be determined here). Let  $L = Tk$  be the length of a twisted ribbon with a twist period  $T$ , and a bending moment  $M$  deforms it in the  $xz$  plane (Figure 2a); thus vectors  $M$  at the free ends of the fibril will be collinear to the  $y$  axis. Dividing the ribbon into segments  $dx$ , we can rewrite eq 1 into

$$dU = \frac{M^2 dx}{2D'(x)}$$

The value  $dU$  is then the energy stored in a small segment  $dx$ , and  $D'(x) = EI'(x)$ , where  $I'(x)$  is the local area moment of inertia in a vicinity of this segment. It is possible to show that this local moment of inertia can be defined as a function of the twist angle  $\theta$  (Figure 2a, inset)<sup>27</sup>

$$I'(\theta) = I_y \cos^2 \theta + I_z \sin^2 \theta - I_{yz} \sin 2\theta$$

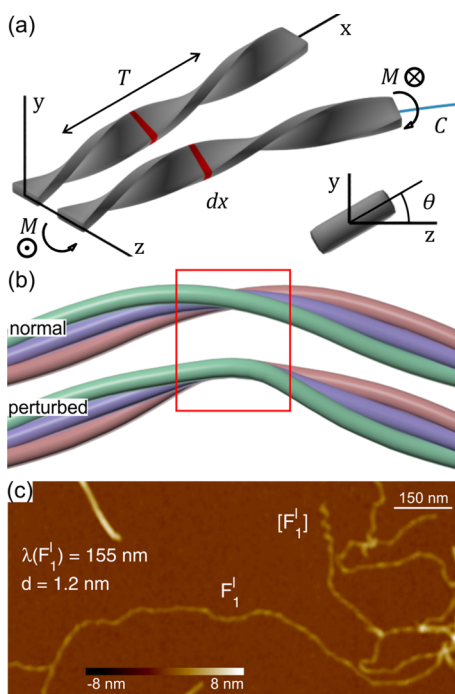


**Figure 2.** (a) Three-dimensional schematic representation of a twisted ribbon bending. (b) Normal (top) and perturbed state (bottom) of the twisted ribbon's filaments. (c) AFM image of flexible BSA fibrils (type  $F_1^l$ ) and a transient helical ribbon polymorphic state  $[F_1^l]$ .

where  $I_{yz} = \int AyzdA$  is a product moment of inertia. From a geometrical relation  $\theta = (2\pi x)/T$ , meaning that  $dx = d\theta \cdot T/2\pi$ , it leads to

$$dU = \frac{M^2}{2E} \frac{T}{2\pi} \frac{d\theta}{I_y \cos^2 \theta + I_z \sin^2 \theta - I_{yz} \sin 2\theta}$$

Taking the integral along  $k$  twists (from  $\theta = 0$  to  $\theta = 2\pi k$ ) and substituting  $Tk = L$ , we get

$$U = \frac{M^2 L}{2E \sqrt{I_y I_z - I_{yz}^2}} \quad (2)$$

For a symmetrical rectangular cross section  $I_{yz} = 0$  and comparing eq 2 to the analogue relation for a simple bar, eq 1, we can see that the average (effective) second moment of inertia in the case of a twisted ribbon is

$$\langle I \rangle = \sqrt{I_y I_z} \quad (3)$$

Although there have been several alternative ways reported to estimate the effective area moment of inertia of a twisted ribbon—with acceptable degrees of success in matching experimental results—the expression provided by eq 3 has not been considered before in the literature. In some works, an arithmetic mean value was used;<sup>14,32,33</sup> in some others, the minimal area moment of inertia was preferred, based on minimal energy considerations and scaling laws.<sup>29,30</sup> As we will see further, this new consideration improves the correlation between results from nanoindentation

and statistical estimation of the persistence length. Here we should investigate more details the consequences of eq 3 applied to the model twisted ribbon amyloids offered by  $\beta$ -lactoglobulin<sup>30</sup> and, in particular, how the persistence length depends on the number of constitutive protofilaments. For the sake of simplicity and clarity, we will use the rectangular cross section of the ribbon, while a model with  $n$  cylindrical protofilaments packed in-line is considered in the Supporting Information; despite this small difference, the same conclusions can be drawn in both scenarios.

**Persistence Length versus Number of Protofilaments.** The area moment of inertia with respect to the principal axes  $y$  and  $z$  of a rectangular cross section with a width  $nd$  and a height  $d$  ( $n$  being number of protofilaments,  $d$  their edge size) are  $I_y = n^3 d^4/12$  and  $I_z = nd^4/12$ , so that  $\langle I \rangle = n^2 d^4/12$ . Because of the well-known relation which connects fibril's propensity to bend, that is, the persistence length  $\lambda$ , with its mechanical properties<sup>34</sup>

$$\lambda = \frac{D}{k_B T} = \frac{E\langle I \rangle}{k_B T} \quad (4)$$

we can deduce that

$$\lambda \sim n^2 \quad (5)$$

This expression is somewhat intermediate between the predictions based on the minimal area moment of inertia, giving  $\lambda \sim n$ , and those based on the arithmetic averaging, giving  $\lambda \sim (n^3 + n)/2$ . Yet, this result remains true provided that all protofilaments keep their exact positions along each other and form regular, undisturbed twists (Figure 2b, top). However, the strength of interaction between protofilaments must be weaker than between  $\beta$ -sheets inside the core. A slight rearrangement in vicinities of points with the smallest second moment of inertia and highest curvature (Figure 2b, bottom) can lead to concentration of bending around these points, and then a more general relation than eq 5 should be applied

$$\lambda \sim n^\nu \quad (6)$$

where  $2 \geq \nu \geq 1 + \delta$  depending on how strong these mentioned interactions differ. In the case of free relative sliding, but with protofilaments remaining attached (i.e., without increase of degrees of freedom), we obtain the critical case of bending only with respect to the lowest second moment of inertia and  $\nu \rightarrow 1 + \delta$ , where the vanishingly small parameter  $\delta > 0$  takes into account an energy increase through the additional elastic bending of protofilaments due to rearrangement. The best fit of the data on 218 fibrils<sup>29</sup> with eq 6 gives  $\nu \approx 1.3$  (Figure S3), which illustrates the predictive power of the proposed theoretical approach. Yet, the difference in the quality of the fit with  $\nu = 1$  (the lower boundary arising from the assumption of lowest energy bending, i.e., bending versus the smallest area moment of inertia) and  $\nu = 1.3$  is very small, which shows that, although the

generalized eq 6 form can possibly better describe the persistence length *versus* number of filaments at larger numbers *n*, for the most frequently encountered cases with low *n*, the minimum energy bending assumption remains a robust approach.

For various types of amyloid fibrils adsorbed on mica (including the bovine serum albumin fibrils studied here), a 3/4 self-avoiding random walk exponent has been found experimentally,<sup>18,33</sup> which demonstrates equilibration on the substrate, following directly from Flory's energy minimization arguments. Hence, we can now apply this approach to estimate the Young's moduli of both BSA and  $\beta$ -lactoglobulin twisted ribbon fibrils.

Left-handed double-protofilament BSA twisted ribbons, previously identified as polymorph type F<sub>1</sub>, have a persistence length of  $\lambda \approx 155$  nm based on 296 tracked fibrils and protofilament diameter *d* = 1.2 nm (Figure 2c).<sup>18</sup> For a cross section of two circular protofilaments,  $I_z = \pi d^4/32$  and, using the parallel axis theorem,  $I_y = 5\pi d^4/32$ . According to eqs 3 and 4,  $\langle I \rangle = 0.456$  nm<sup>4</sup>,  $D = 0.64 \times 10^{-27}$  Pa m<sup>4</sup>, which together with the possibility of the filaments' lateral sliding and reorganization (eq 6) leads to an elastic modulus in the range of  $E \approx 1.4$ –3 GPa. This result is in perfect agreement with nanoindentation measurements reported previously for the rigid BSA fibrils ( $E = 3.0 \pm 0.6$  GPa)<sup>31</sup> that possess a nanotube conformation but identical elastic modulus.

In the case of  $\beta$ -lactoglobulin, it is possible to go even further in Young's modulus estimation because this system provides us data for a different number of protofilaments. Indeed, the fitting equation can be reduced to a form  $\lambda = n'\pi d^4 E / 64k_B T$  (eq S6), with  $n' = 1.3$  in this particular case (Figure S3). The final value  $E = 4.0$  GPa is much closer to the results of nanoindentation measurements ( $E = 3.7 \pm 0.8$  GPa)<sup>31</sup> than the value obtained by only considering the smallest area moment of inertia ( $E = 4.98$ ).<sup>29</sup>

**Bending of a Helical Ribbon.** In order to extend this approach to a helical ribbon, we need to find maximal and minimal values of area moment of inertia of its cross section. With a good level of precision, we can approximate the cross section with a sector of a ring centered at the position described by the angle  $\theta$  (Figure 3). The sector angle  $\varphi$  is constant along the helical ribbon. Thus, angle coordinates of the ribbon's edges can be described by two parametric helices delayed by  $d' = nd/\cos\alpha$ , along the parameter *x*, where *nd* is the ribbon's width, that is, by the two equations  $\varphi_1(x) = 2\pi x/T + \varphi_0$  and  $\varphi_2(x) = 2\pi(x - d')/T + \varphi_0$ . Hence

$$\varphi = \varphi_1 - \varphi_2 = \frac{2\pi}{T} \frac{nd}{\cos\alpha} \quad (7)$$

The maximum area moment of inertia for a ring segment is obtained at  $\theta = 0$  and equals  $I_{\max} = \int_{-\varphi/2}^{\varphi/2} \sin^2 \gamma \, d\gamma \cdot \int_{r_1}^{r_2} r^3 \, dr = (\varphi + \sin \varphi)(r_2^4 - r_1^4)/8$ . At  $\theta = \pi/2$ , it gets to

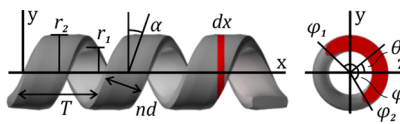


**Figure 3.** Three-dimensional schematic representation of a helical ribbon's geometrical parameters upon bending. The element of a ribbon *dx* approximated with a ring sector shape (sector angle  $\varphi$ ) with a center position defined by the angle  $\theta$ .

the minimum value  $I_{\min} = \int_{-\varphi/2}^{\varphi/2} \cos^2 \gamma \, d\gamma \cdot \int_{r_1}^{r_2} r^3 \, dr = (\varphi - \sin \varphi)(r_2^4 - r_1^4)/8$ . These expressions, together with eq 3, lead to

$$\langle I \rangle = \frac{r_2^4 - r_1^4}{8} \sqrt{\varphi^2 - \sin^2 \varphi} \quad (8)$$

where  $\varphi$  is defined by eq 7.

We can now benchmark predictions of eqs 7 and 8 on the experimental case of the end-capped heptapeptide  $\text{CH}_3\text{CONH-}\beta\text{A}\beta\text{AKLVFF-CONH}_2$ , for which all the structural parameters needed are known and published.<sup>19,31</sup> By taking  $d' = 45$  nm,  $r_2 = 4$  nm,  $r_2 - r_1 = 1.7$  nm,  $T = 110$  nm, and  $\lambda = 14.7$   $\mu\text{m}$ , we obtain  $D = 61 \times 10^{-27}$  Pa m<sup>4</sup>,  $\langle I \rangle \approx 60$  nm<sup>4</sup> and, finally, the Young's modulus of 1 GPa, which is very close to the range of 1.7–2.9 GPa measured by nanoindentation.<sup>31</sup> In view of the homogeneous cross section and prismatic profile approximations taken in eq 1 and eq 8, this can only lead to an overestimation of the average area moment of inertia here, so this agreement is found to be remarkably good.

**Bending of a Nanotube.** Equation 8 is derived with the assumption that the helices do not interact with each other on their sides (in the extreme scenario with  $\varphi \rightarrow 2\pi$ , this assumption does no longer hold). An opposite situation occurs in the closed nanotube bending scenario (Figure 1d and Figure 4a), where the interaction between helices plays a crucial role and will shift the position of the neutral axis (Figure 4a, bottom) away from the central axis. We further assume that the helices are kept together by adhesion forces between side chains of the  $\beta$ -sheet fibril's core in the regions under tension, driven by line tension energy reduction,<sup>22</sup> while material in compression regions behave as in a full-shell nanotube case. In the case of equality of tension and compression energy density, we recover the lowest boundary for shift values of the neutral axis, such as the homogeneous nanotube case. However, adhesion and compression forces in a closed helical ribbon, assimilated to a nanotube, will likely contribute in a different way. Hence, the adhesion forces act on one side of neutral axis which is shifted by distance *a* from the central line of the nanotube, so that they equilibrate the moment of compression forces. Thus, the parameter *a* embodies the asymmetry of contributions to the total stored energy arising from compression and adhesion (*a* = 0 nm for the fully symmetric case, *i.e.*, a homogeneous nanotube).

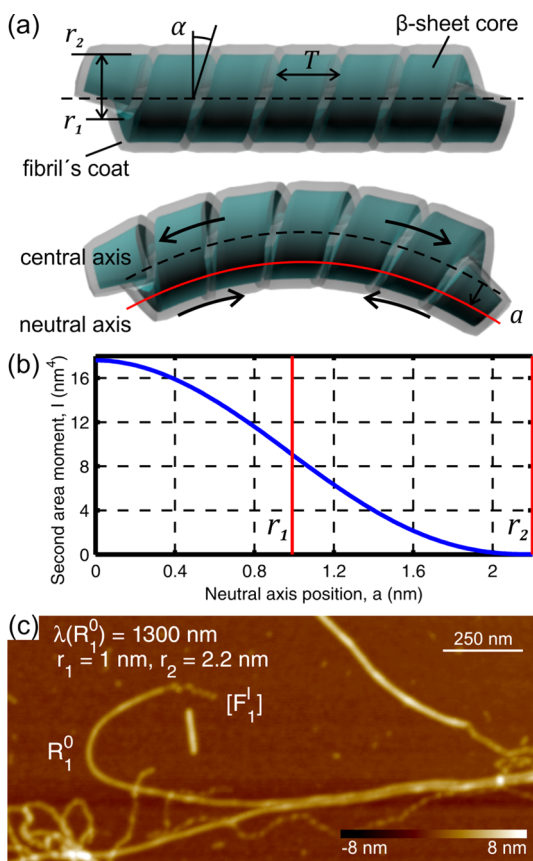


**Figure 4.** (a) Three-dimensional schematic representation of a nanotube bending. The moments of adhesion forces above and compression forces below the neutral axis equilibrate each other. (b) Dependence of the second moment of inertia  $I$  on neutral axis position  $a$  (eq S7) with  $r_1 = 1$  nm and  $r_2 = 2.2$  nm that are radii of the BSA fibrils  $R_1^0$  type. (c) AFM image of the type  $R_1^0$  BSA rigid fibrils. Note that one end of the fibril has a transient helical ribbon conformation  $[F_1]$ .

We present an exact solution to this problem in Supporting Information, and the resulting dependence between the area moment of inertia  $I$  and the neutral axis position  $a$  of a nanotube is plotted in Figure 4b for BSA fibrils of type  $R_1^0$  as an example. Using the known persistence length  $\lambda \simeq 1300$  nm based on 121 tracked fibrils and the elastic modulus  $E \simeq 1.4\text{--}3$  GPa, we can estimate  $D = 5.38 \times 10^{-27}$  Pa m<sup>4</sup> via eq 4 and

$I \simeq 1.8\text{--}3.8$  nm<sup>4</sup>. The consequent estimated values of  $a$  lay in a range of 1.4–1.6 nm (Figure 4b). This can explain the apparent discrepancy between Young's moduli of flexible and rigid BSA fibrils when taking a simplistic full-shell nanotube geometry for the closed nanotubes with a ring cross section and hence  $I = \pi(r_2^4 - r_1^4)/4$ . Indeed, in that case for the elastic modulus of the rigid  $R_1^0$  BSA fibrils, one would get  $I = 17.613$  nm<sup>4</sup> (the same value can be obtained assuming  $a = 0$  nm via eq S7, or  $\varphi = 2\pi$  via eq 8) and an unrealistic  $E \simeq 0.31$  GPa, which is one magnitude lower than that estimated for the flexible fibrils and that measured from direct nanoindentation results.<sup>31</sup>

## CONCLUSIONS

In summary, we have described a general approach to solve the challenging task of quantifying nanomechanical properties of various polymorphic forms of amyloid fibrils based on the theory of elasticity<sup>27</sup> and statistical analysis of fibrils' coordinates extracted from AFM images.<sup>18,30,31</sup> The exact expression for the area moment of inertia has been derived for twisted helical ribbons and nanotubes, allowing extraction of Young's moduli, which are in excellent agreement with experimental findings from nanoindentation measurements. The present approach pushes forward the analysis of nanoscale mechanics of protein fibrils. For example, in the case of the nanotubes formed from closure of helical ribbons, one can recover the correct estimation of Young's modulus by duly quantifying the shift in the neutral axis caused by different energetic contributions of the adhesive and compressive parts of the nanotubes under bending. The current and more simplistic assumption of a perfectly axisymmetric cross section (ring-shaped homogeneous section) in this case would lead to an unrealistic estimation of the elastic modulus of at least 1 order of magnitude lower. These results illustrate that the polymorphic shape of the amyloid fibrils needs to be carefully considered in order to extract reliable Young's moduli.

The main findings of the article are summarized in Table 1.

## MATERIALS AND METHODS

**Preparation of Fibrils.** Details on the preparation of  $\beta$ -lactoglobulin and end-capped heptapeptide  $\text{CH}_3\text{CONH-}\beta\text{A}\beta\text{AKLVFF-CONH}_2$  fibrils are reported elsewhere.<sup>19,29–31</sup> Bovine serum albumin fibrils were obtained by dissolving 1.5 g of the protein in 23.5 mL of Milli-Q water adjusted to pH 2 with HCl. The protein (Sigma-Aldrich, product no. A7030, lyophilized powder  $\geq 98\%$ ) was dialyzed using a semipermeable membrane (Spectra/Por dialysis membrane 1, MWCO 6–8 kDa) for 3 days prior to the incubation. A vessel containing the resulting 6 w/w % protein solution was kept in an oil bath at high temperature (90 °C). Mild agitation was applied throughout the whole incubation process. Samples taken after 40 and 100 h were visualized by AFM.

**Atomic Force Microscopy.** All samples were diluted to the BSA concentration 0.1 w/w % with pH 2 Milli-Q water. Then 20  $\mu\text{L}$  aliquots of solution were deposited onto freshly cleaved mica. After 2 min, each substrate was rinsed with Milli-Q water and dried with an air flow. AFM scanning was performed with a MultiMode VIII scanning probe microscope (Bruker, USA) operated in a tapping mode under ambient conditions.

**Height and Persistence Length Estimation.** Bovine serum albumin fibrils' data were extracted from high-resolution AFM images with dimensions of  $15 \times 15 \mu\text{m}$  and a resolution of  $5120 \times 5120$  pixels. Statistical analysis of fibrils' average height and persistence length estimation via end-to-end distance versus internal contour length and bond correlation function were conducted using an in-house software written in MATLAB.<sup>18</sup> In this study, we neglect errors on the height estimation from AFM images

**TABLE 1. Effective Area Moment of Inertia  $\langle I \rangle$  for Different Polymorphic forms As Derived in the Present Article**

polymorphic form	effective area moment of inertia $\langle I \rangle$
general averaging <sup>a</sup>	$\langle I \rangle = \sqrt{I_y I_z - I_{yz}^2}$
twisted ribbon <sup>b</sup>	$\langle I \rangle = \frac{n^2 d^4}{12}$
twisted ribbon <sup>c</sup>	$\langle I \rangle = \frac{\pi n^2 d^4}{64} \sqrt{\frac{4}{3} - \frac{1}{3n^2}}$
twisted ribbon <sup>d</sup>	$\langle I \rangle \approx \frac{\pi n^2 d^4}{64}$
helical ribbon	$\langle I \rangle = \frac{r_2^4 - r_1^4}{8} \sqrt{\varphi^2 - \sin^2 \varphi}$ , where $\varphi = \frac{2\pi}{T} \frac{nd}{\cos \alpha}$
nanotube <sup>e</sup>	$\langle I \rangle(a) = \left[ a \left( \frac{r^2}{2} + a^2 \right) \sqrt{r^2 - a^2} + r^2 \left( \frac{r^2}{2} - 2a^2 \right) \arccos \left( \frac{a}{r} \right) \right]_{\max(a, r_1)}^{r_2}$

<sup>a</sup>  $I_{yz} = 0$  if  $y$  or  $z$  is an axis of symmetry. <sup>b</sup> Rectangular cross section with a width  $nd$  and a height  $d$ . <sup>c</sup> Composed of  $n$  protofilaments with a diameter  $d$ . <sup>d</sup> Composed of  $n$  protofilaments with a diameter  $d$ , assuming the possibility of their lateral sliding. <sup>e</sup> As a function of a neutral axis shift  $a$  (see Figure 4).

because we expect that the broadening of the height distribution due to errors from microscopy measurements is more significant than the effect of the actual variation in height along fibril contours and also because the averaging was carried out on a large statistical data set, leading to an accurate estimation of height averages. It should be noted that deviations from the average height can affect the extrapolated elastic modulus  $E$  due to the power 4 dependence of the area moment of inertia  $I$ . For example, in the case of flexible BSA twisted ribbons with  $\langle I \rangle = 0.456 \text{ nm}^4$  and the average diameter of a protofilament  $d = 1.2 \text{ nm}$ , the error of the average diameter  $\Delta d = 0.1 \text{ nm}$  might lead to  $\Delta \langle I \rangle = 0.15 \text{ nm}^4$ , corresponding to about 33% change in elastic modulus value. Thus, these errors remain within the range of uncertainties associated with errors from nanoindentation measurements.

*Conflict of Interest:* The authors declare no competing financial interest.

*Acknowledgment.* The authors acknowledge support from the Swiss National Science Foundation (SNF) (2-77002-11).

*Supporting Information Available:* Brief commentaries for the pure bending of a transversally loaded beam; exact solution for the twisted ribbon persistence length on number of protofilament,  $n$ , dependence; area moment of inertia vs neutral axis position for a nanotube. This material is available free of charge via the Internet at <http://pubs.acs.org>.

## REFERENCES AND NOTES

- Tan, S. Y.; Pepys, M. B. Amyloidosis. *Histopathology* **1994**, *25*, 403–414.
- Dobson, C. M. Protein Misfolding, Evolution and Disease. *Trends Biochem. Sci.* **1999**, *24*, 329–332.
- Selkoe, D. J. Folding Proteins in Fatal Ways. *Nature* **2003**, *426*, 900–904.
- Dobson, C. M. Protein Folding and Misfolding. *Nature* **2003**, *426*, 884–890.
- Caughey, B.; Lansbury, P. T. Protofibrils, Pores, Fibrils, and Neurodegeneration: Separating the Responsible Protein Aggregates from the Innocent Bystanders. *Annu. Rev. Neurosci.* **2003**, *26*, 267–298.
- Chiti, F.; Dobson, C. M. Protein Misfolding, Functional Amyloid, and Human Disease. *Annu. Rev. Biochem.* **2006**, *75*, 333–366.
- Eisenberg, D.; Jucker, M. The Amyloid State of Proteins in Human Diseases. *Cell* **2012**, *148*, 1188–1203.
- Zhang, S. G. Fabrication of Novel Biomaterials through Molecular Self-Assembly. *Nat. Biotechnol.* **2003**, *21*, 1171–1178.
- Knowles, T. P. J.; Buehler, M. J. Nanomechanics of Functional and Pathological Amyloid Materials. *Nat. Nanotechnol.* **2011**, *6*, 469–479.
- Cherny, I.; Gazit, E. Amyloids: Not Only Pathological Agents but Also Ordered Nanomaterials. *Angew. Chem., Int. Ed.* **2008**, *47*, 4062–4069.
- Gras, S. L. Surface- and Solution-Based Assembly of Amyloid Fibrils for Biomedical and Nanotechnology Applications. *Adv. Chem. Eng.* **2009**, *35*, 161–209.
- Li, C.; Adamcik, J.; Mezzenga, R. Biodegradable Nano-composites of Amyloid Fibrils and Graphene with Shape-Memory and Enzyme-Sensing Properties. *Nat. Nanotechnol.* **2012**, *7*, 421–427.
- Marshall, K. E.; Serpell, L. C. Structural Integrity of Beta-Sheet Assembly. *Biochem. Soc. Trans.* **2009**, *37*, 671–676.
- Smith, J. F.; Knowles, T. P. J.; Dobson, C. M.; MacPhee, C. E.; Welland, M. E. Characterization of the Nanoscale Properties of Individual Amyloid Fibrils. *Proc. Natl. Acad. Sci. U.S.A.* **2006**, *103*, 15806–15811.
- Nelson, R.; Sawaya, M. R.; Balbirnie, M.; Madsen, A. O.; Riekel, C.; Grothe, R.; Eisenberg, D. Structure of the Cross- $\beta$  Spine of Amyloid-like Fibrils. *Nature* **2005**, *435*, 773–778.
- Wegmann, S.; Medalsy, I. D.; Mandelkow, E.; Müller, D. J. The Fuzzy Coat of Pathological Human Taufibrils Is a Two-Layered Polyelectrolyte Brush. *Proc. Natl. Acad. Sci. U.S.A.* **2012**, *110*, E313–E321.
- Knowles, T. P.; Fitzpatrick, A. W.; Meehan, S.; Mott, H. R.; Vendruscolo, M.; Dobson, C. M.; Welland, M. E. Role of Intermolecular Forces in Defining Material Properties of Protein Nanofibrils. *Science* **2007**, *318*, 1900–1903.
- Usov, I.; Adamcik, J.; Mezzenga, R. Polymorphism Complexity and Handedness Inversion in Serum Albumin Amyloid Fibrils. *ACS Nano* **2013**, *7*, 10465–10474.
- Adamcik, J.; Castelletto, V.; Bolisetty, S.; Hamley, I. W.; Mezzenga, R. Direct Observation of Time-Resolved Polymorphic States in the Self-Assembly of End-Capped Heptapeptides. *Angew. Chem., Int. Ed.* **2011**, *50*, 5495–5498.
- Adamcik, J.; Mezzenga, R. Proteins Fibrils from a Polymer Physics Perspective. *Macromolecules* **2012**, *45*, 1137–1150.

21. Ziserman, L.; Lee, H. Y.; Raghavan, S. R.; Mor, A.; Danino, D. Unraveling the Mechanism of Nanotube Formation by Chiral Self-Assembly of Amphiphiles. *J. Am. Chem. Soc.* **2011**, *133*, 2511–2517.
22. Lara, C.; Handschin, S.; Mezzenga, R. Towards Lysozyme Nanotube and 3D Hybrid Self-Assembly. *Nanoscale* **2013**, *5*, 7197–7201.
23. Castelletto, V.; Hamley, I. W.; Cenker, C.; Olsson, U. Influence of Salt on the Self-Assembly of Two Model Amyloid Heptapeptides. *J. Phys. Chem. B* **2010**, *114*, 8002–8008.
24. Oda, R.; Artzner, F.; Laguerre, M.; Huc, I. Molecular Structure of Self-Assembled Chiral Nanoribbons and Nanotubules Revealed in the Hydrated State. *J. Am. Chem. Soc.* **2008**, *130*, 14705–14712.
25. Lamour, G.; Yip, C. K.; Li, H.; Gsponer, J. High Intrinsic Mechanical Flexibility of Mouse Prion Nanofibrils Revealed by Measurements of Axial and Radial Young's Moduli. *ACS Nano* **2014**, *8*, 3851–3861.
26. Ling, S.; Li, C.; Adamcik, J.; Shao, Z.; Chen, X.; Mezzenga, R. Modulating Materials by Orthogonally Oriented  $\beta$ -Strands: Composites of Amyloid and Silk Fibroin Fibrils. *Adv. Mater.* **2014**, *26*, 4569–4574.
27. Timoshenko, S. *Strength of Materials*; D. Van Nostrand Company, Inc.: New York, 1948.
28. Usov, I.; Adamcik, J.; Mezzenga, R. Polymorphism in Bovine Serum Albumin Fibrils: Morphology and Statistical Analysis. *Faraday Discuss.* **2013**, *166*, 151–162.
29. Adamcik, J.; Berquand, A.; Mezzenga, R. Single-Step Direct Measurement of Amyloid Fibrils Stiffness by Peak Force Quantitative Nanomechanical Atomic Force Microscopy. *Appl. Phys. Lett.* **2011**, *98*, 193701.
30. Adamcik, J.; Jung, J. M.; Flakowski, J.; Rios, P. D. L.; Dietler, G.; Mezzenga, R. Understanding Amyloid Aggregation by Statistical Analysis of Atomic Force Microscopy Images. *Nat. Nanotechnol.* **2010**, *5*, 423–428.
31. Adamcik, J.; Lara, C.; Usov, I.; Jeong, J. S.; Ruggeri, F. S.; Dietler, G.; Lashuel, H. A.; Hamley, I. W.; Mezzenga, R. Measurement of Intrinsic Properties of Amyloid Fibrils by the Peak Force QNM Method. *Nanoscale* **2012**, *4*, 4426–4429.
32. Sachse, C.; Grigorieff, N.; Fändrich, M. Nanoscale Flexibility Parameters of Alzheimer Amyloid Fibrils Determined by Electron Cryo-Microscopy. *Angew. Chem., Int. Ed.* **2010**, *49*, 1321–1323.
33. Lara, C.; Usov, I.; Adamcik, J.; Mezzenga, R. Sub-Persistence-Length Complex Scaling Behavior in Lysozyme Amyloid Fibrils. *Phys. Rev. Lett.* **2011**, *107*, 238101.
34. Manning, G. S. Polymer Persistence Length Characterized as a Critical Length for Instability Caused by a Fluctuating Twist. *Phys. Rev. A* **1986**, *34*, 668–670.